s-Nebula : Novel Spin-Based Building Blocks for Advanced TeraHertz Applications

Document Title	Characterization of the first generation pulsed THz emitters		
Document type	Deliverable D1.2	**Authors**	Mathias Vanwolleghem (CNRS-IEMN) Henri Jaffrès (CNRS-UMPhy) Sukhdeep Dhillon (CNRS-LPENS)
Due date	31/12/2020	**Dissemination level**	Public
Project	s-Nebula	**Grant number**	863155
Coordinator	THALES SA	**Project coordinator**	Dr. Romain Lebrun
Call identifier	H2020-ICT-2019-2020		
Work Package	**WP1 : Spin-based THz Emitters (STE)**		
Project Start date	01/01/2020		
Project Duration	42 months		

Beneficiaries list

No	Name	Short name	Country
1	THALES SA	THALES	France
2	CENTRE NATIONAL DE LA RECHERCHE SCIENTIFIQUE CNRS	CNRS	France
3	FRAUNHOFER GESELLSCHAFT ZUR FOERDERUNG DER ANGEWANDTEN FORSCHUNG E.V.	Fraunhofer	Germany
4	JOHANNES GUTENBERG-UNIVERSITAT MAINZ	JGU	Germany
5	FREIE UNIVERSITAET BERLIN	FUB	Germany
6	VYSOKA SKOLA BANSKA - TECHNICKA UNIVERZITA OSTRAVA	VSB	Czech Republic
7	UPPSALA UNIVERSITET	UU	Sweden

Contents

This project has received funding from the European Union's Horizon 2020 research and innovation programme under grant agreement No 863155

1. Overview D1.2: Characterization of the first generation pulsed THz emitters

1.1 Deliverable and relation to WP1 tasks

Characterization of a first generation of active metallic THz emitters based on transition metal/heavy metal bilayers (typically Co/Pt bilayers) using terahertz time domain spectroscopy (TDS) with detected fields equivalent or larger than standard electro-optical materials. The output performances will be characterized in both reflection and transmission modes over the spectral bandwidth of the TDS system. The optimal parameters in terms of emitter growth, excitation powers and pulse width will be investigated.

1.2 Partners involved

CNRS-UMPhy, CNRS-LPENS, CNRS-IEMN, Thales, FUB, VSB.

1.3 Project Resources used and how provided by sNebula

- IEMN TDS setup (preexisting instrument)
- IEMN sputter deposition Leybold (consumables and running costs provided by sNEBULA budget)
- FUB TDS setup (preexisting setup)
- LPENS TDS setup (preexisting setup)

1.4 Key results

Investigation of THz spintronic emitters based on several materials with two types of spin-to-charge conversion mechanisms:

- *Inverse spin-Hall effect (ISHE° based THz spintronic emitters:*
    - *Benchmarking of THz-TDS setups using standard metallic heterostructures (W/Co/Pt) from JGU,*
    - *Demonstration of efficient THz emission with ferromagnetic Heusler alloys,*
    - *Fine tuning of the magnetic anisotropies in rare-earth metal allows is compatible with efficient THz emission whilst providing a full polarization control,*
- *Rashba interfaces based THz spintronic emitters:*
    - *Barrier height in LAO/STO is detrimental for efficient THz emission,*
    - *Preliminary and promising results on topological insulators based THz emitters presents interconversion efficiency similar to metallic systems.*

This project has received funding from the European Union's Horizon 2020 research and innovation programme under grant agreement No 863155

2. Results & Accomplishments

Deliverable 1.2 presents the results of the systematic study of the different material systems for optically driven pulsed spintronic THz emitters. This is specifically aimed at investigating viable alternatives for the record interfaces based on the SO-driven inverse spin Hall effect in 3d/4d and 3d/5d systems (specifically Co/Pt). The performances are, where possible, compared to the THz emission obtained via optical rectification on nonlinear EO materials (ZnTe) and to that of a record reference ISHE sample provided by JGU/FUB (that has been extensively characterised and reported in literature [Seifert, Tom, et al. "Efficient metallic spintronic emitters of ultrabroadband terahertz radiation." Nature photonics 10.7 (2016): 483-488.]:
MgO[2nm]/Pt[2nm]/$Co_{20}Fe_{60}B_{20}$[1.8nm]/W[2nm]/sapphire[substr] (hereafter designated STE_REF). Such a structure has been provided to each of the partners in June 2020.
Two main classes are investigated as optically driven STEs: ISHE systems & Rashba systems. 4 partners have been involved in this deliverable: CNRS-IEMN, CNRS-LPENS, CNRS-UMPhy, Thales. Each of them has characterized a selection of the available emitters on their own respective THz-TDS systems with its own characteristics (in terms of available power, pulse duration and repetition rate). Where possible these performances have been compared to those of the STE_REF.

a. Characterization setups

This preliminary section describes the specifics of the different setups used.
IEMN: the TDS setup at IEMN is **not** wideband. It is limited by the 100fs pulse duration of the fs laser (Coherent MaiTai) used and by the bandwidth of the gated detector (dipole photoconductive antenna on a LT-GaAs substrate with a cutoff frequency around 6 THz). No electrooptic detection is implemented in the IEMN setup. The average power provided by the 80MHz fs laser is 3.2W with a central wavelength at 820nm. The pump IR power is controlled by variable attenuators. A **typical average pumping power of 100mW is used**. A total delay of up to 1ns can be covered by the delay line in steps of 10 fs. The setup has been extended with an electromagnet providing up to 0.1 T magnetic bias that can be controlled in-plane. In order to allow for polarization dependent measurements, two $\pm$45° relative oriented wire-grid polarizers have been added to allow via sum and difference measurements the contributions of two orthogonal polarizations. The emitter can be probed in reflective and transmissive configuration. In the reflective configuration, the orientation of the applied magnetic field can be controlled in-plane. In transmission configuration this extension is under construction (**Fig.a.1**)

This project has received funding from the European Union's Horizon 2020 research and innovation programme under grant agreement No 863155

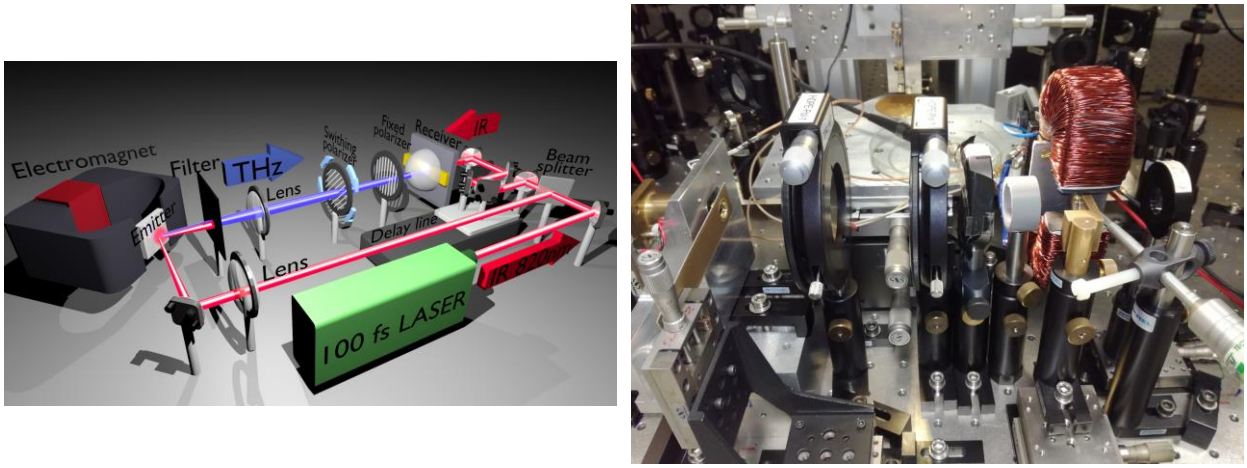

Fig.a.1 *Setups built at IEMN. In reflection (left) both the applied magnetic field and the sample orientation with respect to it can be controlled. In transmission configuration (right) the orientation of the magnetic applied field is fixed.*

LPENS/UMPhy/Thales: the TDS setup is based on a 100fs coherent oscillator using electro-optic sampling for THz pulse detection. The average power provided by the pump laser is 1 W with a central wavelength at 800nm and repetition rate of 76 MHz. The system is arranged in reflection mode to study the THz spin emitters where the optical pump excites the spintronic surface without going through the substrate and the emitted THz is collected from the same surface. A typical average pumping power of 200mW is used. A total delay of a few hundred picoseconds can be covered by the delay line in steps of typically 30fs. A small permanent magnet is used to apply the magnetic field. A system with a 15fs oscillator is currently being built to extend the THz detection bandwidth.

b. Results

Ultrafast spin-to-charge conversion (SCC) is responsible for the emission of linearly-polarized THz electromagnetic dipolar radiation. SCC is made possible owing to the spin–orbit interactions (SOI) near or at interfaces between a ferromagnet (FM) and an active material characterized by a large atomic number Z with strong SOI such 4*d as* (Pd) or **5*d*** (Pt, W, Ta, Au:Pt, Au:W, Au:Ta) heavy metal (HM)that we have investigated here in WP1. Ultrafast SCC emitters possess the advantage of being phonon-less, resulting in the absence of any THz spectral dips, even at room temperature, and allowing extremely large unperturbed emission bandwidths (larger than 20 THz) compared to other technologies based on femtosecond oscillators.

Investigated extensively in the quasi-static excitation regime using ferromagnetic resonance (FMR) and spin-pumping (SP) techniques, SCC may occur *via* the inverse spin-Hall effect (ISHE) owing to an asymmetric deflection of the spin trajectory induced by SOIs. Moreover, SCC may also arise from the inverse Edelstein–Rashba effect (IREE) **[2]** that occurs at spin–orbit split Rashba interfaces states like in Bi/Ag or $LaAlO_3/SrTiO_3$ systems. Such conversion was recently experimentally demonstrated on Rashba surface states **[3-4]** and on surface states of topological insulators (TI) **[5-6]** in the THz domain and explain the strong interest for those materials like $Bi_{1-x}Sb_x$ alloys investigated here. However, the physics of (inverse) spin-Hall effects and (inverse)

This project has received funding from the European Union's Horizon 2020 research and innovation programme under grant agreement No 863155

Edelstein effects differs from that, in spin-Hall one probes the spin-flow of carriers, whereas in Rashba systems one probes the spin-polarization or the spin-accumulation. This makes the problem pretty different once one considers the emission of THz waves, in particular because spin-orbit at interfaces, like Rashba fields, are to be avoided in spin-Hall owing to the spin-memory loss whereas has to be involved for the Edelstein conversion.

In an international context, HM and Rashba materials have shown large THz emissivity comparable to and even larger than that realized using mature nonlinear crystals such as ZnTe. Such emission properties are generally probed using a standard THz-TDS setup. The FM/HM junction, where Fe/(Pt,W), Co/(Pt,W) or CoFeB/(Fe,W) represents the best candidates, exploits the ISHE with the so-called spin Hall angle (SHA). This represents the ratio between the transverse charge current $\mathbf{j_c}$ generated over the spin-current $\mathbf{j_s}$ source, as the main figure of merit of the local SCC. When summed over the active thickness of layers, SCC scales with a characteristic length, the product of the spin-Hall angle (SHA) with the spin-diffusion length l_{sf} (SDL), that lies around 0.2 nm for Co/Pt TMs. In the time-domain, this length matches the total volume of the transient dipole charge oscillations responsible for the dipolar emission.
Beyond, the aforementioned spintronic structures are being extensively investigated for their spin–orbit torque (SOT) properties required for magnetic commutation functionalities. Progress in these materials is concentrated, in particular, on interface engineering for the optimization of the spin transmission to reduce the energy consumption. This goal is in order to significantly reduce the interfacial spin-loss due to unwanted local spin-orbit fields as recently shown experimentally and more recently via first-principles calculations in the case of 3d/5d systems. The efficiency of spin-transmission scales now with the electronic transmission, characterized as the surface conductance or spin-mixing conductance of the considered interface. The anatomy of spin-current injection in transition metal based multilayers can be investigated using combined spin-pumping/FMR and THz-TDS mesurements.
In this deliverable, we thus first investigated in details standard metallic heterostructures used for THz emission, evidencing the key parameters behind the THz emission and the role of the electronic transmission between transition metal and metallic ferromagnets (CNRS-UMPhy, CNRS-LPENS). In parallel, we finely tuned the properties of ferromagnetic metals in order to tune their magnetic anisotropies (CNRS-IEMN), which is key for future polarization functionalities, whilst maintening high THz emission. Furthermore, we investigated alternative approaches for THz emission based on 2DEG and topological insulators. Very recent experiments by FMR spin-pumping/ISHE methods foresaw a possible breakthrough for THz emission supplied by Rashba-states exhibiting IEE characteristic lengths of 6 nm ($LaAlO_3/SrTiO_3$) **[7]** and ($Al_2O_3/SrTiO_3$) **[8]** thus largely exceeding the one of Co/Pt **[9]**, or using topological insulators [10]**.**

b.1. ISHE systems

The different ISHE systems that have been characterised can be classified along

1. standard 5*d* systems
2. Au-alloyed spacer systems
3. rare-earth allloy systems

This project has received funding from the European Union's Horizon 2020 research and innovation programme under grant agreement No 863155

b.2 Rashba systems

1. NiFe/(ALO,LAO)/STO Rashba systems
2. Co/BiSb topological Insulator (TI) systems

The next paragraphs describe the results on each of these with a particular attention to a comparison of the performance with respect to reference emitters.
We discuss our main results concerning the THZ-TDS spectra based on respective:

- **3*d*/5*d* heavy metals and alloys** (Co/Pt, NiFe/Au:W, NiFe/Au:Ta) **[11-13]**
- **Rashba-based interfaces** ($LaAlO_3/SrTiO_3$ – $Al_2O_3/SrTiO_3$) **[7-8]**
- **Co/$Bi_{0.79}$ $Sb_{0.21}$ topological insulators**.

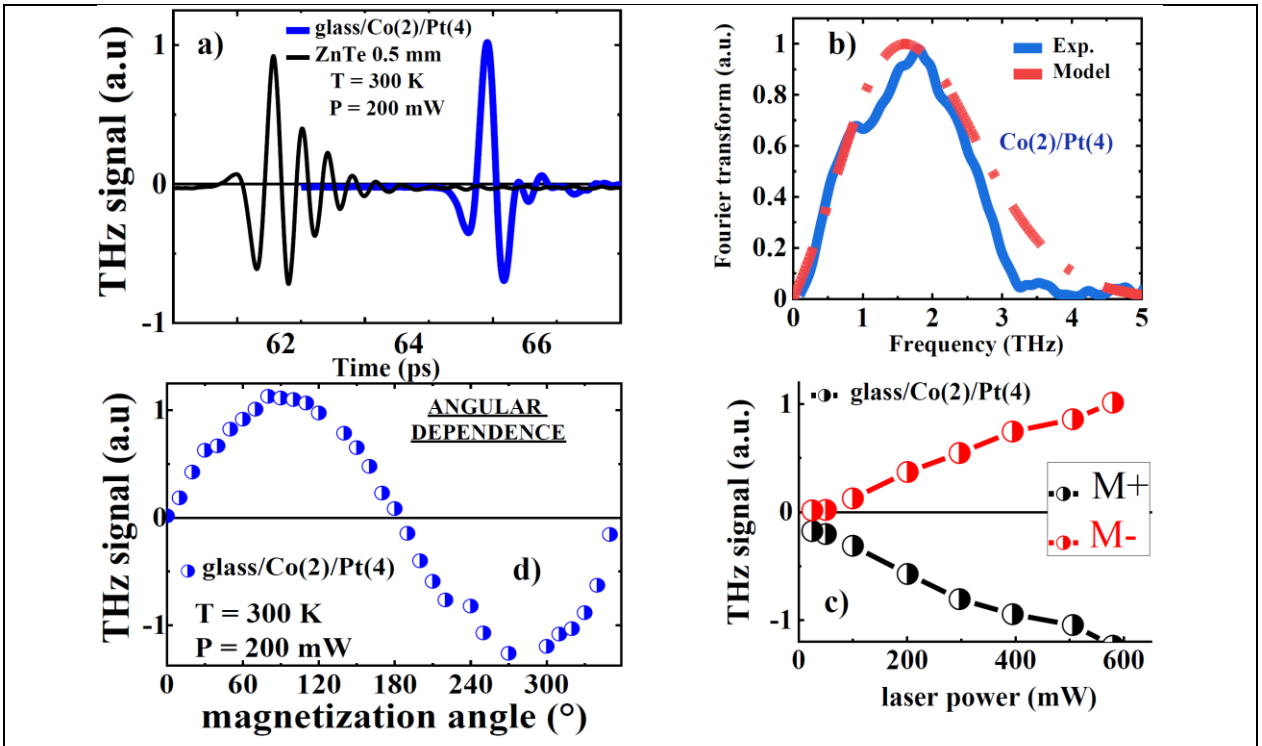

FIG.b.1.1.1 *(a) Temporal THz emission acquired using THz-TDS at room temperature on Co(2)/Pt(4) system under a 100- fs laser pulse with average power of P=200 mW. Comparison is shown with THz emission from ZnTe crystal via optical rectification under the same experimental conditions. (b) Fourier transform of the Co(2)/Pt(4) temporal signal giving the spectrum in the [0- 3] THz window (blue). Comparison with the modeling using parameters described in the text (red dashed line). (c) Amplitude of the maximum THz wave vs laser power excitation in the [0-600] mW range, repetition rate of 80 MHz, and under two different opposite magnetic polarities. (d) Characteristic sine angular dependence of the THz-wave amplitude by varying the in-plane Co magnetization angle.*

b.1 ISHE systems

The results and analyses are strongly connected to deliverable D3.1 dealing with modeling and analyses of THz-TDS spectra. This contribution presented below has given rise to the publication

This project has received funding from the European Union's Horizon 2020 research and innovation programme under grant agreement No 863155

of an article in Applied Physics Review journal published in December 2020: *TH Dang et al., Appl. Phys. Rev 7, 041409 (2020)* **[1].**
In particular, in this first subsection, we will explore the different capability of transition-metal based couple materials in terms of magnetic polarization (Co vs. NiFe), spin-Hall angle (**SHA for Pt=0.1 vs. SHA for Au:W =0.15 and SHA for Au:Ta alloys=0.45**) and resistivity (**resistivity of Pt=20 µOhm.cm and resistivity of Au:Ta and Au:W=80-90 µOhm.cm**) and spin-transmission in order to determine the general trends for THz output optimization.

b.1.1 standard ISHE 3d/4d-5d heavy metallic systems

Using THz-TDS, we have demonstrated a sizable spin-charge conversion and subsequent THz emission from transition metal (NiFe, Co)/Pt bilayers in the sub-picosecond timescale after excitation by a 100 fs pulse laser. In both case of NiFe and Co used as spin injectors, the performances exceed the ones of ZnTe electro-optical materials in the same experimental condition (**Fig.b.1.1.1a**) for Co and **Fig.b.1.1.2a** for NiFe). The Fourier transform of the spectra (**Fig.b.1.1.1b**) within the 0-3THz window exhibits the characteristic shape expected from a far-field dipolar radiation source origin and it is remarkably fitted by our numerical modelling (**WP3**) involving spin-dependent electronic diffusion in the FM/HM bilayers, spin-dependent reflections at interfaces (inner and outwards) and momentum and spin-relaxation.
Moreover, in the whole set of experiments, the THz emission was shown to be controlled by the direction of the magnetization in the plane of the FM layer revealing the ISHE origin and the THz signal is proportional to the laser pump power (**Fig.b.1.1.1d**).

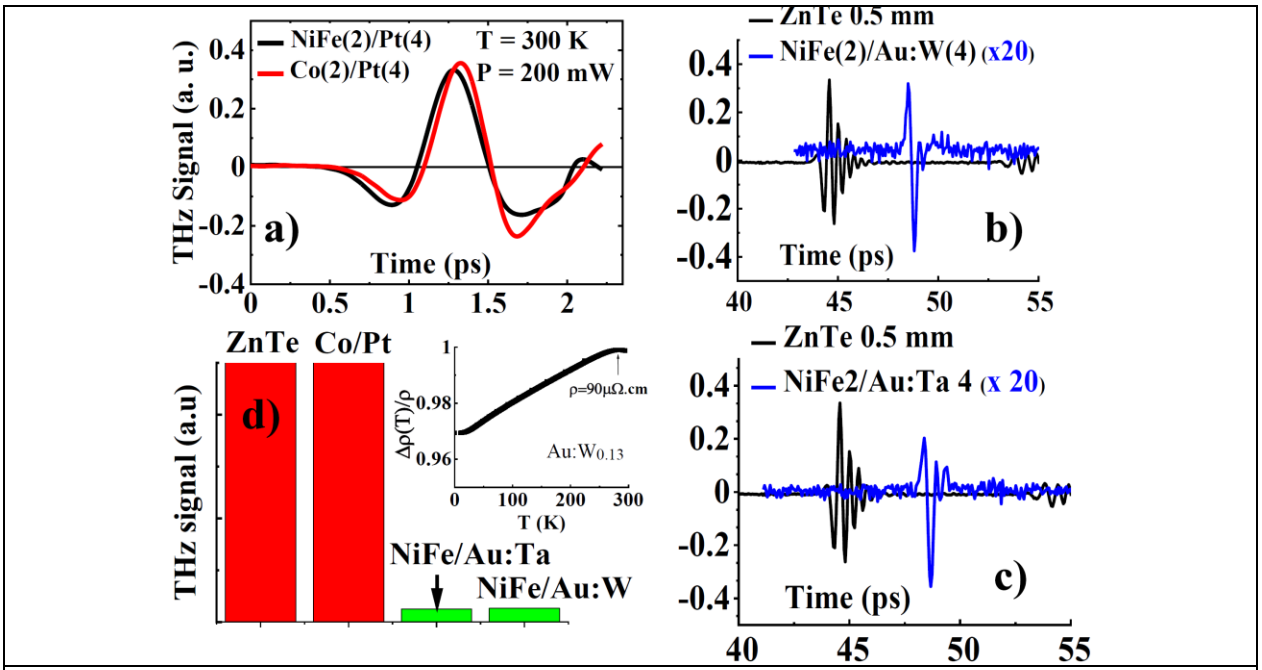

FIG.b.1.2.1 *(a) Comparison of the THz emission at room temperature (P=200 mW) acquired on Co(2)/Pt(4) and NiFe(2)/Pt(4) samples showing similar features and equivalent amplitudes. (b) and (c) Emission of NiFe/Au:(W,Ta) systems compared with ZnTe(110) crystal. Measurements taken at room temperature under a laser fluence of*

This project has received funding from the European Union's Horizon 2020 research and innovation programme under grant agreement No 863155

P=200 mW. (d) Peak-to-peak amplitude comparison between the well-known THz emitter ZnTe(110) and spintronic-based emitters including the reference Co/Pt and NiFe/Au(W,Ta) systems. Inset of (d) Temperature variation of the resistivity of Au:$W_{0.13}$ from 300 to 10 K showing a small decrease in 3%. The sample Au:$W_{0.13}$ corresponds to a typical resitivity of 90 µOhm.cm at RT for an approximate W content of about 13%.

b.1.2 Au-based alloy spacer and sink configurations in 3*d*/4*d*-5*d* heavy metallic systems

The Au:W and Au:Ta alloys with a content of W=0.13 and content of Ta =0.05 giving rise to respective spin-Hall angle of 0.15 for Au:W and 0.45 for Au:Ta was shown to only display a smaller THz signal (**Fig. b.1.2.1b and Fig. b.1.2.1c**) reduced by a factor 20 compared to Co/Pt despite a larger spin-Hall angle than Pt (spin-Hall angle of 0.1). This particular feature of THz signal drop in the alloy series originates from several causes that we discuss below in term of spin-transmission and material resistivity.

In order to understand those points, we extensively used the FMR spin-pumping/ISHE method to correlate the spin-injection temporal dynamics to the steady regime of spin-injection. In order to reveal the major role played by the electronic transmission on THz, our aim was to point out the strong correlation between the THz emission power to the efficiency of spin-charge conversion obtained in radio frequency (rf) spin-pumping experiments. We demonstrated that the THz emission power (in units of the electric field E_{THz}), displaying sequential electronic events, is proportional to an overall figure of merit, i.e the product of spin-Hall angle times the spin-transmission times the spin-diffusion length. By FMR methods, we could extract the spin-transmission via the spin-conductance. We then proved that the transmission in NiFe/Au-based samples was reduced (typically by one order of magnitude) compared to Co/Pt systems which actually represent the state-of-the art in term of materials due to its strong electronic transmission, and in particular for the majority spin channel.

Moreover, despite an expected smaller optical absorption in Au-based alloys due to a smaller conductivity of those materials compared to Pt, the correlated higher resistivity in alloys is associated to a smaller efficiency of spin-charge interconversion and then to a smaller THz emission owing to more efficient electronic current relaxation. This was clearly put in evidence by comparing both NiFe/Pt and NiFe/Au-based alloy spectra (**Fig.b.1.2.1**). These experimental results were confirmed in the theory works performed in WP3, in which we modeled such mechanisms by advanced ab initio methods and simplified finite difference time-domain simulations (FDTD). In the next period, we will investigate how spin sink could permit to improve the electronic transmission in some of these heterostructures. In parallel, metallic ferromagnets with higher spin polarization such as Heusler alloys will be considered.

b.1.3 rare-earth FM alloys and multilayers: $TbCo_2$/FeCo

IEMN has concentrated on demonstrating the potential offered by rare-earth Tb-based alloys with two objectives in mind:

- Exploiting the strong in-plane magnetic uniaxial anisotropy. It was pointed out in [**14**] that a multilayer combination of TbCo and FeCo thin layers leads to an effective FM layer with low saturation fields (order of 100Oe) and high anisotropy, through exchange coupling. Using FeCo/TbCo2/FeCo as the FM layer in the STE would therefore allow StonerWolfarth magnetization rotation in the FM layer by only varying the hard axis bias.

This project has received funding from the European Union's Horizon 2020 research and innovation programme under grant agreement No 863155

- verifying a possible contribution of the strong spin-orbit effect of the heavy rare earth (providing a potential extra ISHE effect). This latter effect is still under study and requires growth of pure TbCo emitters.

All samples provided by IEMN have been grown in a Leybold Z550 radio-frequency (RF) diode sputter deposition system, with a base vacuum of 3.10-7mbars. Argon pressures during the deposition are in the 10-3mbar range. The different layer thicknesses were controlled by adjusting the angular speed of the rotary turntable substrate holder in an oscillation mode under the chosen target. The magnetization loops were characterized using an ADE-EV9 vibrating sample magnetometer (VSM), after a careful calibration and with a large averaging value for each magnetic field value, considering the 18Å thickness of the ferromagnetic layer.

In all samples, the thicknesses of the Pt and W layers are chosen to be equal to those of the optimized STE_REF: 2nm. It was pointed out by Seifert **[15]** that the total metal thickness presents an optimum depending on the materials used. This model was later refined by Torosyan **[16]** to take into account the individual FM and NM layer thicknesses and their conductivities on the efficiency of the THz generation. Making a reasonable assumption that the conductivity of a FeCo/$TbCo_2$/FeCo multilayer is not radically different from that of the amorphous $Co_{20}Fe_{60}B_{20}$ alloy in the STE_REF, and all the rest being equal it makes sense to chose a total thickness for the multilayer equal to that of the amorphous CoFeB: 1.8nm. Furthermore, in a first step the relative amount of FeCo and TbCo layers have been chosen to be quasi-identical and symmetrically distributed in the ML: FeCo(5Å)/$TbCo_2$(8Å)/FeCo(5Å). The only other varied parameter has been the substrate material on which these Tb-based emitters have been grown: float glass, sapphire, Si, and SiOx on Si. By their varying refractive index and THz absorption, as well as their IR pump transparency, they will influence the efficiency of the emission.

It was verified by VSM that the developed Tb-based ML has approximately the same saturation magnetization M_s of approximately 200 μemu as the CoFeB. All the rest being equal, similar levels of spin pumping are therefore expected, and therefore similar THz signals. This is confirmed in **Fig.b.1.3.1a** for the emitters characterized in a 45° reflection configuration (see **Fig.a.1** for the setup details). The sample code used here is as follows. The 5213 series are Tb-based multilayers; the 5211 series are emitters where the FM layer is a single pure CoFe with the same thickness (1.8nm). The extra letter indicates the substrate type (S: sapphire; I: Si; O: SiOx/Si; G: float glass). The last number is an internally used indication referring to the measurement number. It can be concluded that the peak-to-peak signal is about the same as the STE_REF delivered by FUB (sample name 48OGX01) only when an oxidized Si substrate is used. The ML on sapphire (i.e. the same substrate as STE_REF) has approximately 50% V_{pp}. This seems to indicate that the two extra interfaces in the FM multilayer induce some spin loss. The stronger emission on oxidized Si might come from THz reflection on the Si substrate. This has to be further investigated. On the other hand, for a pure CoFe emitter on sapphire (not exhibiting any extra interfaces leading to potential spin loss) we still observe a slight reduction of $0.7V_{pp,STE\_REF}$. This also needs further investigation.

This project has received funding from the European Union's Horizon 2020 research and innovation programme under grant agreement No 863155

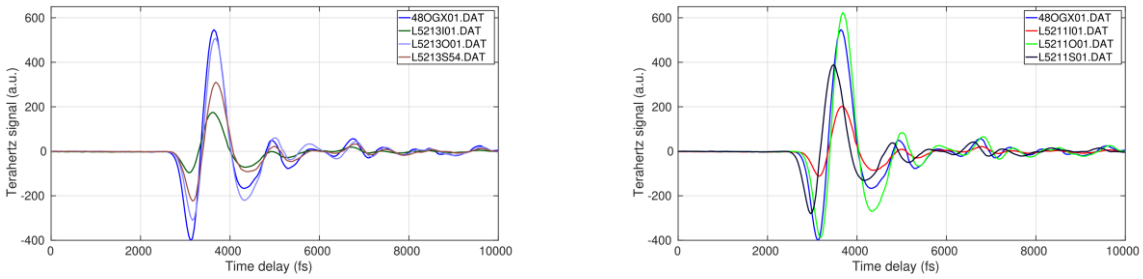

***Fig b.1.3.1**: Comparison of then THz performance of Tb-based emitters and CoFe emitters to the reference CoFeB emitter (48OGX01) in a reflection configuration. The sample codes are detailed in the text.*

The best STE emitters (STE_REF & 5211 on SiOx/Si) have been compared to a standardly used emitter in reflection configuration. The photo-Dember effect in InAs has been known to lead to the emission of powerful THz pulses upon excitation with IR pulses in reflection **[17]**. **Fig. b.1.3.2** illustrates that under identical excitation conditions, the best STEs attain approximately 20% of peak-to-peak field strength. In a first estimation this indicates that STEs in reflection have about 14dB absolute power loss with respect to InAs[1]. However, they clearly outperform InAs with respect to bandwidth, as can be seen from the approximately three times shorter THz pulse.

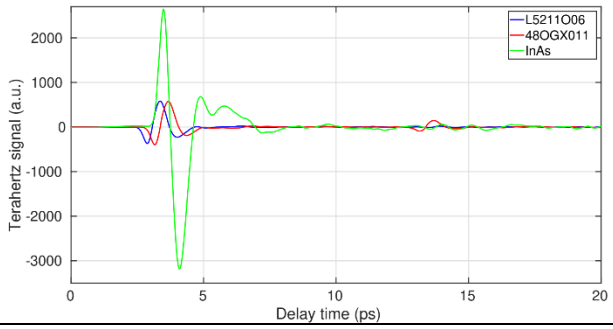

***FIG b.1.3.2:** Best pulsed emitters compared to photoDember on InAs*

Obviously, a direct improvement can be obtained by operating the STEs in transmission, which is impossible for InAs emitters due their heavy free carrier absorption of THz radiation. Moreover, in InAs the photoDember dipole is oriented perpendicular to the surface. The dipole radiation pattern is therefore suboptimal for easy THz collection with a lens. In a STE the the induced fast transient charge dipole is in in plane (perpendicular to the magnetization). It therefore radiates maximally perpendicular to the dipole. A transmission excitation will therefore maximally allow THz collection. **Fig. b.1.3.3** shows the obtained temporal traces in transmission on the Tb-based emitters (compared to the STE_REF). The IR excitation is from the metallic side so that the THz pulse is collected through the substrate. Not only does this avoid echos moreover it avoids IR pump loss in the substrate.

1 The absolute power that can be obtained from InAs in this configuration is estimated to be not higher than 100nW (estimated from the values reported in [SarukuraJAP1998] under scaled pumping conditions. Work is underway to measure these absolute THz pulse powers.

This project has received funding from the European Union's Horizon 2020 research and innovation programme under grant agreement No 863155

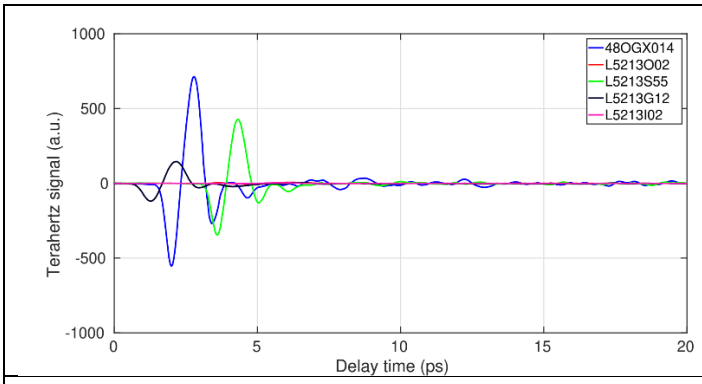

Fig b.1.3.3: *comparison of Tb-based transmitters measured in transmission to the reference STE_REF. All emitters are pumped from the metal side, suppressing the echo. The float glass emitter L5213G suffered from strong degradation due to thermal effects. Apart from the sapphire substrate emitter, all other emitters are hindered by THz absoprtion in the substrate.*

It is immediately obvious that the V_{pp} is increased by at least 50% as compared to the reflection configuration, approaching the power of InAs emitters. Again it is noted that the extra interfaces induce power loss probably due to spin losses. It is also obvious that the Si substrates (5213I and 5213O) absorb the emitted THz pulses. The STE on float glass suffer from thermal issues due to low thermal conductivity of the glass substrate leading to fast degradation of the emitter. The absolute power is still under study. It is expected. Further optimization of the collected THz power is expected by integration of a hemispherical sapphire lens on the sapphire substrate as in **[18]**.

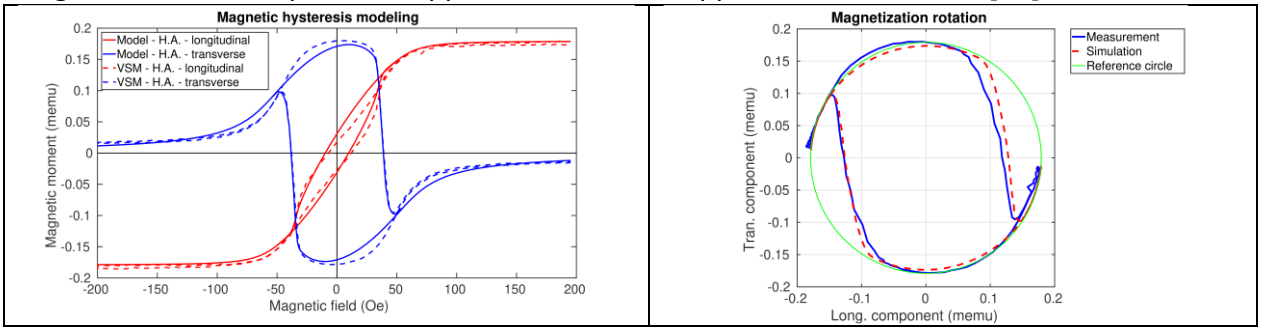

Fig b.1.3.4*: VSM measurements and Stoner Wohlfarth model fit on Tb-based multilayers, illustrating the possibility to obtain a coherent in-plane magnetization rotation over nearly 360°. The polarization of the accompanying THz radiation is predicted to replicate this behavior.*

Finally, some expectations are given regarding the polarization control of Tb-based emitters. By applying a magnetic bias along the hard axis, the VSM measurements show that the magnetization of the FM layer gradually rotates towards the easy axis. At some critical value the competition between the Zeeman energy and the anisotropy energy induces a jump of the magnetization before it completely reverses. This behavior is expected to be reproduced in the THz polarization, since, according to the ISHE physics the radiating dipole is always perpendicular to the local magnetization (or spin polarization). This work will be extensively discussed in the deliverable D1.5 related to task 1.5.

<u>b.2 Rashba systems:</u>

b.2.1 NiFe/(ALO,LAO)/STO Rashba-based THz emission (CNRS-UMPhy, CNRS-LPENS)

Related phenomena to SHE like the Inverse Edelstein Effect occurring at Rashba surface states, like Ag/Bi, $LaAlO_3/SrTiO_3$ (LAO/STO) **[7]** or $Al_2O_3/SrTiO_3$ **[8],** or at the surface of topological insulators like Bi_2Se_3 are presently the subject of numerous studies worldwide in the various spintronic laboratories because of their high SCC efficiency. In more details, quantum

This project has received funding from the European Union's Horizon 2020 research and innovation programme under grant agreement No 863155

phenomenon called the Rashba effect typically occurs at surfaces and interfaces where the spatial symmetry breaking results in a built-in electric potential or field (ε) along the out-of-plane direction $\vec{z}$. The Rashba Hamiltonian is given by $H_R = \alpha_R(\vec{k} \times \vec{\sigma}) \cdot \vec{z}$, where $\vec{\sigma}$ is the vector of the Pauli spin matrices, $\vec{k}$ the momentum and α_R the Rashba coefficient, proportional to the field ε and to the SO interactions. In a Rashba system, the spin degeneracy of the 2D band structure is lifted. A spin current in a Rashba system generates a net charge current giving the IEE effect. The efficiency of IEE may be estimated with its corresponding length as a figure of merit, λ_{IEE}, given by the ratio between the 2D charge current generated (j_c^{2D}) and the 3D spin current injected (j_s^{3D}). λ_{IEE} is proportional to the Rashba coefficient α_R and the relaxation time τ, with $\lambda_{IEE} = \frac{\alpha_R \tau}{\hbar}$. The advantage of the 2D is a strong increase of SCC with SO. λ_{IEE} is to be compared to λ_{SCC} of heavy metals given above. A remarkable example showing Rashba splitting is the interface between STO and LAO where a 2D electron gas (2DEG) may form.

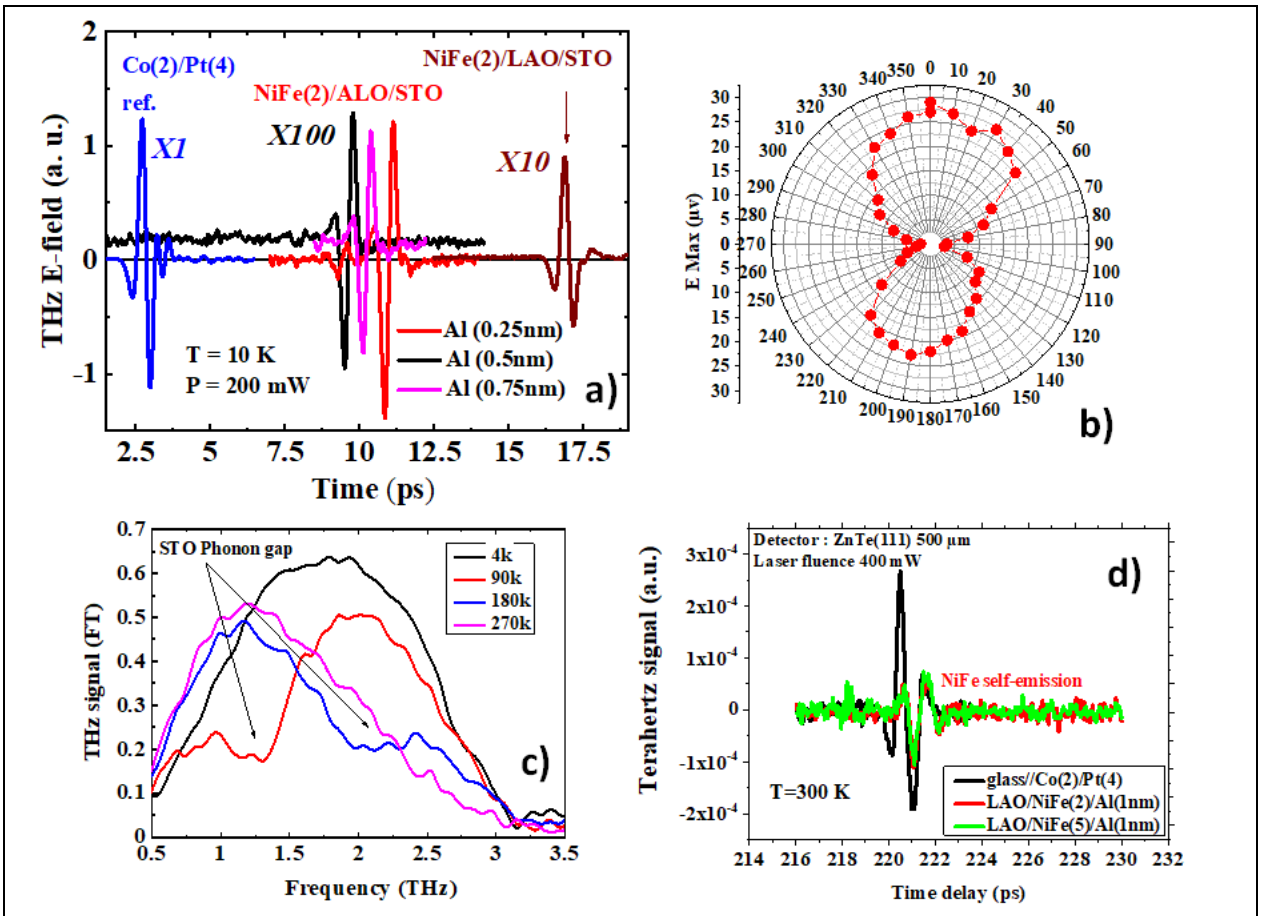

Fig.b.2.1.1 *: a) THz-TDS spectra at room temperature on NiFe(2)/LAO(2u/STO and NiFe(2)/ALO(0.25, 0.5.0.75nm)/STO after excitation by a 100 fs laser pulse. The ref. Co/Pt is also shown in blue. b) E-field polarisation dependence of the output THz waveform corresponding to NiFe/LAO/STO sample. c) Temperature-dependence of the FT of the THz spectra for NiFe/LAO/STO showing the temperature-dependence of the phonon gap. d) Self-THz emission of NiFe(2)/LAO substrate sample showing a sizeble signal.*

Importantly, FMR spin-pumping experiments has revealed that the LAO/STO 2DEGs possesses a sizable Rashba coupling **(α=20 meV.Å)**. From those data and the reduction of the LAO barrier

This project has received funding from the European Union's Horizon 2020 research and innovation programme under grant agreement No 863155

thickness, one could expect an increase of the THz-TDS by one order of magnitude compared to Co/Pt. This finding has recently been extended to the surface of STO and interfaces between STO and metals such as Al. *$SrTiO_3$ 2DEGs:* Using spin-pumping injection, we have recently harnessed the tunable Rashba SO coupling of STO 2DEGs to achieve a SCC with a high efficiency (λ_{IREE}=7 nm), to date the largest ever obtained. The generated charge may be tuned in amplitude and sign by the application of a gate voltage shifting the Fermi level within the Ti 3*d* band. THz-TDS experiments on oxide-based Rashba systems have been performed on different set of samples, namely NiFe(2nm)/LAO(2unit cell uc)/STO and NiFe(2nm)/ALO(0.25, 0.5 and 0.7nm)/STO, in the same experimental conditions that used for transition-metal based interfaces (**Fig.b.2.1.1**). The specificity the sample series is that the different barrier thicknesses have been made the thinnest as possible to optimize the electronic spin-transmission. Data display in each case (**Fig.b.2.1.1a**) a measurable THz-TDS signal which is about 1/20 of the Co/Pt signal for the LAO samples and 1/100 of Co/Pt for ALO/Pt. Note that the 2 orders of magnitude of difference between Co/Pt and Co/MoS2 Rashba-based interface was also obtained previously by another team, however demonstrating a THz occurring via IEE. Each case, the FT of the THz signal is revealed to be of spin-charge interconversion origin from (10K –**Fig.b.2.1.1b**- to 300K –**Fig.b.2.1.1d**-). The THz emission displays the characteristic dipolar field emission shape (**Fig.b.2.1.1c**) representative of the IEE spin-charge interconversion process. However, although that our signal of NiFe/LAO/STO remains larger than the self-emission originating from Co, it remains of the order of magnitude (even smaller) than the self-emission from NiFe/LAO substrate (**Fig.b.2.1.1e**) acquired in the same experimental conditions.
Our main conclusion is that NiFe/(LAO, ALO)/STO Rashba-systems do not show a clear proof of significant spin-charge interconversion in the laser excitation regime because of two main raisons: *i*) the barrier is not enough transmissive even reduced down a fraction of nm and *ii*) the Rashba energy splitting may not be strong enough at higher energy than the Fermi level to allow dynamical spin-charge interconversion. On the other hand, NiFe/LAO was shown to provide a subsequent self -HZ-TDZ signal which may be the demonstration of a sizeable Rashba spin-orbit field at the interface.

b.2.2 Co/BiSb topological Insulator (TI) -based THz emission (CNRS-UMPhy, CNRS-LPENS, Thales)

Currently, there is a considerable interest in the electronic properties and their use of the surface states of topological insulators like present Bi_2Se_3 **[5],** Bi_2Te_3 **[6],** Bi(Se,Te), or $Bi_{1-x}Sb_x$ **[19]** and then occurring at the (111) surface of Bismuth (crystal orientation is defined here with respect to the related rhombohedral unit cell, see **Fig. b.2.2.1a**). Indeed, it was recently shown that ultrafast spin-charge interconversion in the THz time-domain can be demonstrated in both Bi_2Se_3 and Bi_2Te_2 topological insulators covered either directly by a thin Co ferromagnetic layer or by a Co/Bi bilayer as spin reservoir. The signal was clearly demonstrated to be of a spin origin from laser optical pumping, and of the order of or larger than a reference Co/Pt.

In these systems, the spin-charge interconversion mechanism relies on the amount of the spin-polarization or spin accumulation generating at the level of the spin-split interface states owing to the particular topological spin texture of a Rashba-like symmetry. The process is then

This project has received funding from the European Union's Horizon 2020 research and innovation programme under grant agreement No 863155

equivalent to the Inverse Edelstein effect (IEE) previously discussed in the case of the Rashba oxide systems (LAO/STO).

We first grew by molecular beam epitaxy (BBE) different sets of **$Bi_{1-x}Sb_x$** samples of different thicknesses (**from 2.5 to 30nm**) with a fraction **x=0.21** on two types of substrates (BaF_2 and High-Resistive Si) corresponding to two different lattice parameters with 14% mismatch for the later (Si). We observed a typical lattice relaxation parameter from the value of the substrate towards the bulk value of BiSb for a typical transition thickness of 6-7 nm (**Fig.b.2.2.1b** for BaF_2 substrate and **Fig.b.2.2.1c** for Si substrate).

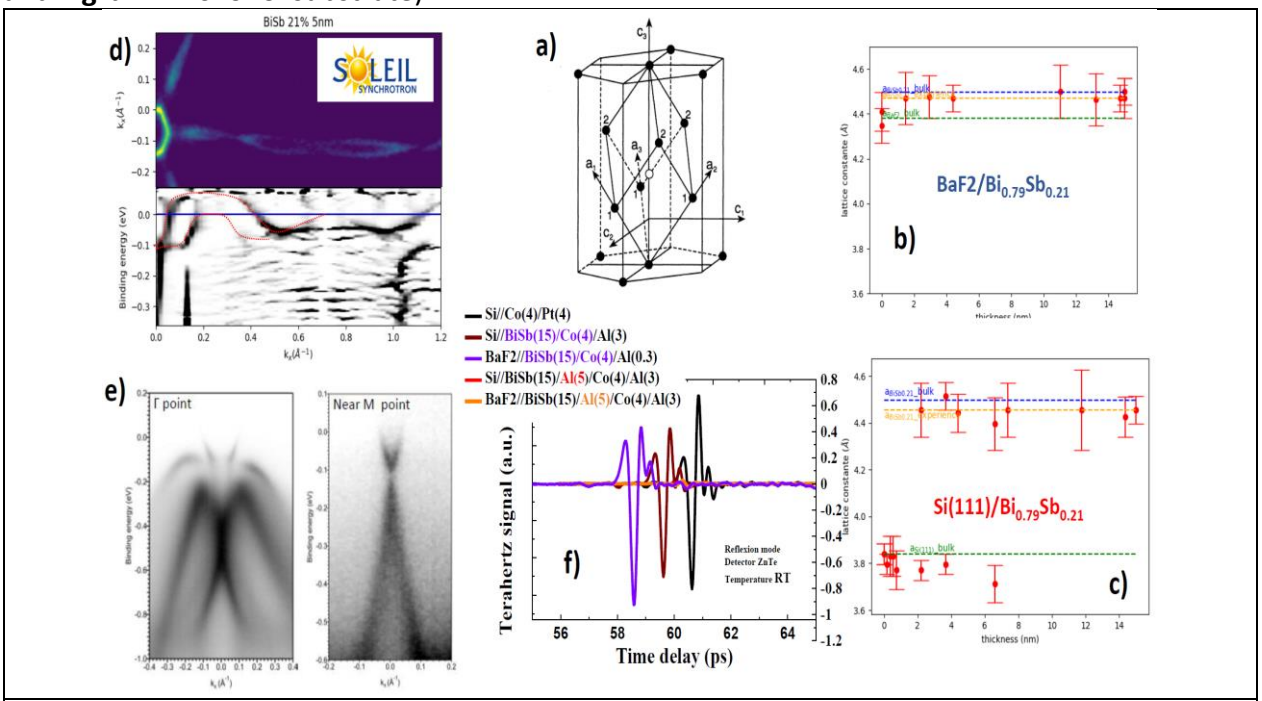

Fig.b.2.2.1 *: a) Rhombohedral crystalline structure of Bi, Sb and $Bi_{1-x}Sb_x$ (topological insulator) structures which unit cell is composed of 6 atomic planes. b) in-plane lattice parameter of $Bi_{1-x}Sb_x$ with x=0.21 and grown on BaF2 extracted from RHEED and showing the lattice relaxation for the thinner BiSb film. c) in-plane lattice parameter of $Bi_{1-x}Sb_x$ with x=0.21 and grown on Si(111) substrate extracted from RHEED and showing the lattice relaxation towards the bulk $Bi_{0.79}Sb_{0.21}$ value for a film thickness of 6 nm. d) ARPES spectroscopy along the Γ-M dispersion line of $Bi_{1-x}Sb_x$ grown on Si(111) the reciprocal space showing the two surface topological states (S1 and S2). e) The typical Rashba-splitting of the Dirac cone observed near the Γ point on the same sample than described in d). e) TDS-THz spectra obtained on different $Bi_{0.79}Sb_{0.21}$ /Co bilayers and on a reference sample (free of Co injector). The BiSb samples are 15nm thick in each case. In magnetic samples (involving Co), the signal is of the order of the Co/Pt THz emitter. The sample free of Co (red and orange) gives no THz emission.*

With Si substrate (Si), we could observe in-situ angular-resolved photoemission spectroscopy (ARPES) evidence of the formation of a characteristic Dirac cone (**Fig.b.2.2.1e**) and the two characteristic surface topological states (S1 and S2) along the Γ-M dispersion and reported on **Fig.b.2.2.1d**. The characteristic spin-texture properties still under investigation via i) combined FMR/spin-pumping, and w-2w harmonic spin-orbit torque experiments and via (ii) tight-binding calculations of the electronic properties.

This project has received funding from the European Union's Horizon 2020 research and innovation programme under grant agreement No 863155

Preliminary THz-TDS measurements shown in ***Fig.b.2.2.1.f*** displays a clear evidence of the THz emission in the time domain from Co/$\mathbf{Bi_{0.79}Sb_{0.21}}$ samples with an amplitude comparable to our best Co/Pt reference THz emitter, highlighting the potential of this approach for efficient THz emission. The THz signal are larger for samples frown on BaF2 substrates. We also observed a sign reversal when reversing the sign of the applied magnetic field, which undoubtedly indicates a spin-injection origin of the THz emission in these promising systems.
In future work, respective bulk and surface states contributions will be discriminated by varying the material thickness.

This project has received funding from the European Union's Horizon 2020 research and innovation programme under grant agreement No 863155

c. Conclusions and Future goals

- Reference s-THz emitters (W/CoFeB/Pt) from JGU show similar and record amplitudes in the different partners laboratories (CNRS-IEMN, CNRS-LPENS, FUB),
- Record emission was equaled for Tb based THz spintronic emitters (CNRS-IEMN), which is key for polarization functionality and for present and future works under investigation in T1.5 and in WP4,
- Co/Pt and CoFeB/Pt based s-THz emitters are to date the most efficient systems among heavy metal/ferromagnet based heterostructures. This was explained by identifying a figure of merit (CNRS-UMPhy, CNRS-LPENS). Undergoing work is planned to improve the interface spin-transmissivity,
- Rashba system based on LAO/STO and ALO/STO does not perform efficiently (CNRS-UMPhy, CNRS-LPENS) due to the oxide barrier that reduces the spin-transmittivity,
- Preliminary results on topological insulator (such as BiSb) shows promising THz emission, and will be investigated further in the next period (CNRS-UMPhy, CNRS-LPENS, Thales).
- Heusler alloys will be investigated due to their high spin-polarization in order to improve the spin-to-charge conversion efficiency (CNRS-UMPhy, CNRS-LPENS, FUB).

This project has received funding from the European Union's Horizon 2020 research and innovation programme under grant agreement No 863155

3. Literature

[1] T. H. Dang et al., Appl. Phys. Rev. 7, 041409 (2020).
[2] V. Edelstein, “Spin polarization of conduction electrons induced by electric current in two-dimensional asymmetric electron systems,” Solid State Communications 73, 233–235 (1990).
[3] C. Zhou, Y. P. Liu, Z. Wang, S. J. Ma, M. W. Jia, R. Q. Wu, L. Zhou, W. Zhang, M. K. Liu, Y. Z. Wu, and J. Qi, “Broadband terahertz generation via the interface inverse Rashba-Edelstein effect,” Phys. Rev. Lett. 121, 086801 (2018).
[4] M. B. Jungfleisch, Q. Zhang, W. Zhang, J. E. Pearson, R. D. Schaller, H. Wen, and A. Hoffmann, “Control of terahertz emission by ultrafast spin-charge current conversion at Rashba interfaces,” Phys. Rev. Lett. 120, 207207 (2018).
[5] X. Wang, L. Cheng, D. Zhu, Y. Wu, M. Chen, Y. Wang, D. Zhao, C. B. Boothroyd, Y. M. Lam, J.-X. Zhu, M. Battiato, J. C. W. Song, H. Yang, and E. E. M. Chia, “Ultrafast spin-to-charge conversion at the surface of topological insulator thin films,” Adv. Mater. 30, 1802356 (2018).
[6] M. Tong, Y. Hu, Z. Wang, T. Zhou, X. Xie, X. Cheng, and T. Jiang, “Enhanced Terahertz Radiation by efficient spin-to-charge conversion in Rashba-Mediated Dirac surface states”, Nano. Letter. Doi:10.1021/acs.nanolett.0c03079 (2020).
[7] E. Lesne, Y. Fu, S. Oyarzun, J. C. Rojas-Sanchez, D. C. Vaz, H. Naganuma, G. Sicoli, J.-P. Attané M. Jamet, E. Jacquet, J.-M. George, A. Barthélémy, H. Jaffrès, A. Fert, M. Bibes, and L. Vila, “Highly efficient and tunable spin-to-charge conversion through Rashba coupling at oxide interfaces,” Nat. Mater.15, 1261–1266 (2016).
[8] D. C. Vaz, P. Noël, A. Johansson, B. Göbel, Fl. Y. Bruno, G. Singh, S. McKeown-Walker, F. Trier, L. M. Vicente-Arche, A. Sander, S. Valencia, P. Bruneel, M. Vivek, M. Gabay, N. Bergeal, F. Baumberger, H. Okuno, A. Barthélémy, A. Fert, L. Vila, I. Mertig, J.-P. Attané, M. Bibes , Nature Materials **18**, 1187–1193 (2019).
[9] J.-C. Rojas-Sanchez, N. Reyren, P. Laczkowski, W. Savero, J.-P. Attané, C. Deranlot, M. Jamet, J.-M. George, L. Vila, and H. Jaffrès, “Spin pumping and inverse spin Hall effect in platinum: The essential role of spin-memory loss at metallic interfaces,” Phys. Rev. Lett. 112, 106602 (2014).
[10] F.Bonell, M. Goto, G. Sauthier, J. F. Sierra, A. I. Figueroa, M. V. Costache, S. Miwa, Y. Suzuki, S. O. Valenzuela, « Control of Spin–Orbit Torques by Interface Engineering in Topological Insulator Heterostructures” Nano Lett. 2020, 20, 8, 5893–5899
[11] P. Laczkowski, J.-C. Rojas-Sanchez, W. Savero-Torres, H. Jaffrès, N. Reyren, C. Deranlot, L. Notin, C. Beigné, A. Marty, J.-P. Attané, L. Vila, J.-M. George, and A. Fert, “Experimental evidences of a large extrinsic spin Hall effect in AuW alloy,” Appl. Phys. Lett. 104, 142403 (2014).
[12]P. Laczkowski, H. Jaffrès, W. Savero-Torres, J.-C. Rojas-Sanchez, Y. Fu, N. Reyren, C. Deranlot, L. Notin, C. Beigné, J.-P. Attané L. Vila, J.-M. George, and A. Marty, “Evaluation of spin diffusion length of AuW alloys using spin absorption experiments in the limit of large spin-orbit interactions,” Phys. Rev.B 92, 214405 (2015).
[13]P. Laczkowski, Y. Fu, H. Yang, J.-C. Rojas-Sanchez, P. Noel, V. T. Pham, G. Zahnd, C. Deranlot, S. Collin, C. Bouard, P. Warin, V. Maurel, M. Chshiev, A. Marty, J.-P. Attané, A. Fert, H. Jaffrès, L. Vila, and J.-M. George, “Large enhancement of the spin Hall effect in Au by side-jump scattering on Ta impurities,” Phys. Rev. B 96, 140405 (2017).
[14] H. Le Gall, J. Ben Youssef, F. Socha, N. Tiercelin, V. Preobrazhensky, P. Pernod, « Low field anisotropic magnetostriction of single domain exchange - coupled (TbFe/Fe) multilayers », Journal of Applied Physics, 87 (9), pp5783-5785 (2000).
[15] Seifert, T., Jaiswal, S., Martens, U., Hannegan, J., Braun, L., Maldonado, P., … Kampfrath, T. (2016). Efficient metallic spintronic emitters of ultrabroadband terahertz radiation. Nature Photonics, 10(7), 483–488. https://doi.org/10.1038/nphoton.2016.91
[16] Torosyan, G., Keller, S., Scheuer, L., Beigang, R., & Papaioannou, E. T. (2018). Optimized Spintronic Terahertz Emitters Based on Epitaxial Grown Fe/Pt Layer Structures. Scientific Reports, 8(1), 1–9. https://doi.org/10.1038/s41598-018-19432-9
[17] Sarukura, N., Ohtake, H., Izumida, S., & Liu, Z. (1998). High average-power THz radiation from femtosecond laser-irradiated InAs in a magnetic field and its elliptical polarization characteristics. Journal of Applied Physics, 84(1), 654–656. https://doi.org/10.1063/1.368068
[18] Papaioannou, E. T., & Beigang, R. (2020). THz spintronic emitters: a review on achievements and future challenges. Nanophotonics. https://doi.org/10.1515/nanoph-2020-0563
[19] D. Hsieh et al., Nature, 452, 06843, (2008)

This project has received funding from the European Union’s Horizon 2020 research and innovation programme under grant agreement No 863155